New Journal of Physics
The open access journal at the forefront of physics

Deutsche Physikalische Gesellschaft DPG IOP Institute of Physics

PAPER • OPEN ACCESS

Bound and stable vortex–antivortex pairs in high-T_c superconductors

To cite this article: J Simmendinger *et al* 2020 *New J. Phys.* **22** 123035

New Journal of Physics
The open access journal at the forefront of physics

Deutsche Physikalische Gesellschaft DPG
IOP Institute of Physics

Published in partnership with: Deutsche Physikalische Gesellschaft and the Institute of Physics

OPEN ACCESS

RECEIVED
21 October 2020

REVISED
25 November 2020

ACCEPTED FOR PUBLICATION
7 December 2020

PUBLISHED
23 December 2020

PAPER

Bound and stable vortex–antivortex pairs in high-T_c superconductors

J Simmendinger[1], M Bihler[1], A M Ionescu[1,2,*], M Weigand[1,3], G Schütz[1] and J Albrecht[4]

[1] Max-Planck-Institute for Intelligent Systems, Heisenbergstraße 3, D-70569 Stuttgart, Germany
[2] National Institute of Materials Physics, Atomistilor 405A, 077125, Magurele, Romania
[3] Helmholtz-Zentrum Berlin für Materialien und Energie GmbH, Institut Nanospektroskopie, Kekuléstrasse 5, 12489 Berlin, Germany
[4] Research Institute for Innovative Surfaces FINO, Aalen University, Beethovenstraße 1, D-73430 Aalen, Germany
[*] Author to whom any correspondence should be addressed.

E-mail: ionescu@is.mpg.de

Keywords: vortex–antivortex pairs, high temperature superconductor, magnetic scanning transmission x-ray microscopy

Individual bound and stable vortex–antivortex (V–AV) pairs in type II superconductors have been imaged using the novel variant of magnetic scanning transmission x-ray microscopy at low temperatures. Hereby the local stray field induced by an individual superconducting flux line locally polarizes a ferrimagnetic sensor layer. We are able to visualize and analyze individual V–AV pairs far below the transition temperature with unprecedented spatial resolution and high contrast. The spontaneous nucleation with a distance of 90 nm occurs at the domain wall (DW) of the ferrimagnetic layer. From their slight deformed structure due to attractive magnetic dipolar-coupling we are able to estimate the binding energy. Our new experimental approach is the first identification of a bound and stable V–AV pair and demonstrates the potential of the x-ray to address vortices in high T_c thin films and heterostructures.

The topology of inhomogeneities in strongly ordered systems defines a very general field of physics [1]. In particular, in condensed matter physics numerous systems with long-range order exhibit local confined structures with particular topology such as vortices, which are categorized by their different vorticity [2, 3]. Controlled creation and manipulation of vortices is of utmost importance for realization of superconducting digital devices [4, 5]. An example is a pair of two one-dimensional superconducting vortices that have clock-wise and counter clock-wise orientation, respectively. Owing to the strong tendency to annihilate the occurrence of bound V–AV pairs is extremely rare. The existence of fluctuation induced V–AV-pairs near the superconducting phase-transition has been theoretically predicted by Kosterlitz and Thouless for (quasi-) two-dimensional geometries [6]. Experimental evidence for this phenomenon have been found in numerous systems by resistance measurements [7–9].

In superconductors decorated with micro-patterned ferromagnets, indications of symmetry-induced coexistence of V and AV have been reported that are generally confined to the sample geometry [10–14]. In ferromagnetic superconductors exhibiting a complex interplay of ferromagnetism and superconductivity studies show a pair-like coexistence of vortices and antivortices in a narrow temperature range [15] but their interaction in these exotic and complex systems remains unexplored.

Over the last decades, real space images of superconducting vortices have been obtained with either scanning mode based techniques such as SQUID-on-tip microscopy [16], magnetic force microscopy [17, 18], scanning Hall-probe microscopy [19], microscopy based on nitrogen-vacancies [20] or Lorentz microscopy [21, 22] with a spatial resolution of less than 100 nm. Spin-polarized scanning tunneling spectroscopy [23] can provide an even higher resolution [24] if the investigated surfaces are flat enough. Technologically relevant high-T_C superconducting films with a high density of outgrowths with heights of several 100 nm restrict the resolution of scanning techniques seriously.

In this work, we use magnetic scanning transmission x-ray microscopy that benefits from the strong dichroic absorption signal (x-ray magnetic circular dichroism, XMCD) at transition metal L edges [25]. For the stray-field imaging [26–29] we use an yttrium iron garnet ($Y_3Fe_5O_{12}$, YIG) lamella cut out of a single crystal by focused ion beam (FIB). With this method it has become possible to image individual superconducting vortices with high spatial resolution of 20 nm and excellent contrast. First direct imaging of bound V–AV pairs stable towards temperatures below T_c and variable external fields has been achieved.

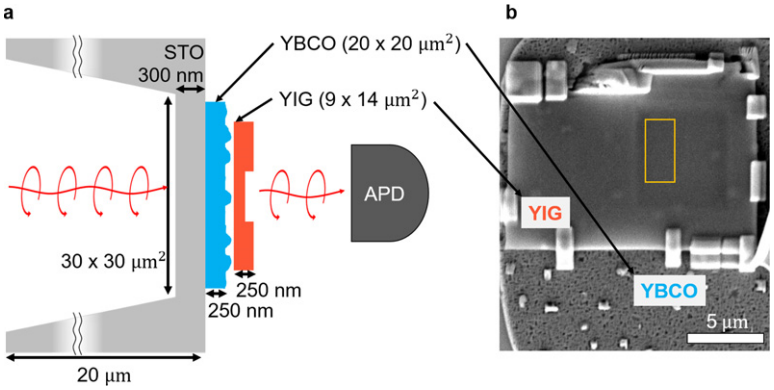

Figure 1. (a) Cross-sectional sketch of the experimental setup. The thickness of the whole sample stack has to be reduced to <1 μm to ensure a sufficient transmission of the soft x-rays, which are detected by an APD. (b) Top view onto the sample stack obtained with SEM. The YIG lamella is glued with titanium stripes on top of the YBCO layer. The orange box marks the region scanned by the x-rays for high resolution imaging.

The nucleation of these stable V–AV pairs is induced by the out-of-plane (OOP) magnetic stray field gradient of a DW of about 100 nm width, formed in an adjacent ferrimagnetic lamella mechanically connected to a superconducting film.

Optimally doped $YBa_2Cu_3O_{7-\delta}$ (YBCO) thin films with a thickness of $d = 250$ nm in combination with a 5 nm $SrTiO_3$ (STO) decoupling layer were grown on single-crystalline STO (001) substrates by pulsed laser deposition.

The YBCO film is nanostructured to 20×20 μm^2 squares using photolithography and ion-beam etching with argon ions. Subsequently, a window (40×40 μm^2) of 300 nm thickness in the substrate has been prepared by mechanical cutting and FIB milling to ensure sufficient transparency in the soft x-ray regime [30].

A YIG lamella of $\sim$250 nm thickness with a lateral size of 9×14 μm^2 was cut out of a YIG single crystal using ion-beam milling techniques [25]. The preparation provides extremely thin lamellas of arbitrary shape while conserving the magnetic properties of the material. The lamellas were mechanically transferred to the YBCO thin film and fixed using Pt deposition. Owing to the strong inflated L edge in iron garnets, an additional window (5×5 μm^2) with a remaining thickness of 100 nm has been cut into the lamella.

The x-ray microscopy measurements are performed at the soft x-ray scanning transmission setup MAXYMUS located at the synchrotron BESSY II of the Helmholtz Center Berlin. The setup reaches a base temperature of 25 K and external magnetic fields of up to $\pm$40 mT with an accuracy of 0.2 mT.

The energy of the x-rays has been tuned to the iron L_3-edge at an energy of 710 eV providing a maximal XMCD contrast of 14%. The monochromatized x-ray beam is focused to a 20 nm spot on the sample and the density distribution as well as the magnetic profile is taken by moving the sample through the scan region. The transmitted intensity is measured using an x-ray sensitive avalanche photodiode (APD).

Figure 1 shows a cross-sectional sketch of the sample stack system and a corresponding SEM image.

The lamella provides two important innovations compared to prior experimental attempts [27, 28]: (i) the defined DW of this soft magnetic lamella produces a strong local stray field gradient, (ii) an outstanding magnetic softness occurs in the DW region. This allows sensing of OOP fields in the mT range such as the stray field of a vortex in the adjacent superconductor first, the sample stack has been cooled through its superconducting transition ($T_c = 88$ K) to a temperature of 26 K in an external magnetic field applied perpendicular to the film plane. The emerging OOP XMCD contrast corresponds to the normalized difference $\frac{I_+ - I_-}{I_+ + I_-}$ of the images taken for opposite x-ray helicity I_+ and I_-. The images in figures 2(c)–(e) are obtained after field cooling in -1 mT, 0 mT, and 2 mT, in which the accuracy of the field strengths was measured to 0.2 mT. The results in the orange marked region of figure 1(b), are exemplarily shown in figure 2 in addition to the density profile $\frac{I_+ + I_-}{2}$.

Common to all three images is a vertically oriented white line corresponding to a magnetic DW in the ferrimagnetic layer of about 100 nm width. It separates two extended domains with a magnetization tilted by 30° OOP as quantitatively determined from the corresponding XMCD contrast (turquoise/yellow area). This magnetization landscape is expected to be induced by mechanical stresses and/or thickness gradients in the thin lamella.

At the DW two circular-shaped spots (red and blue) appear showing the formation of two local fully saturated OOP magnetization regions with opposite direction in the YIG lamella. There are no detectable

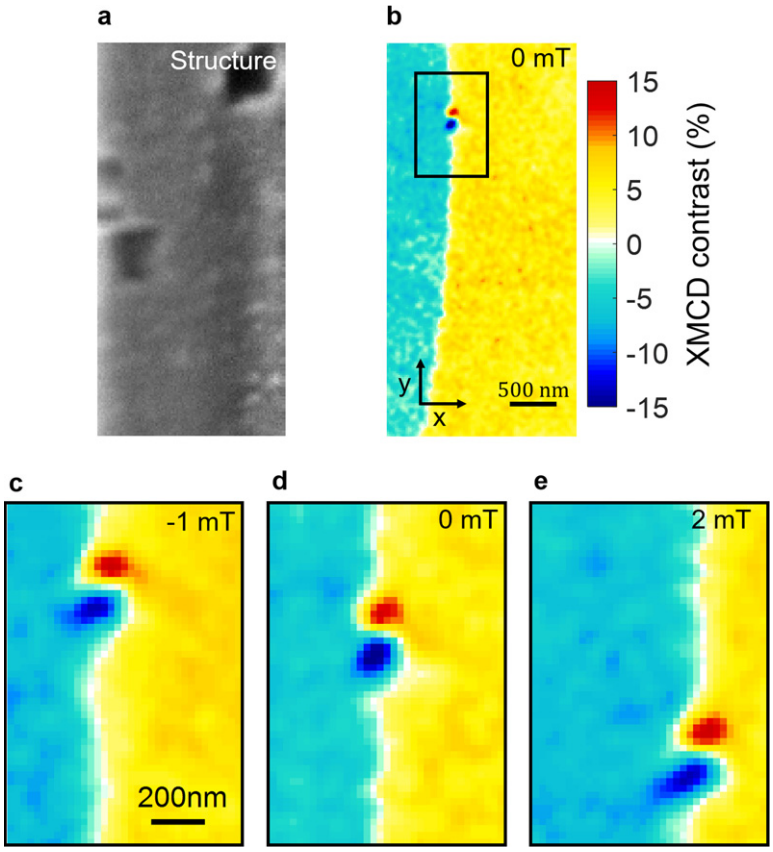

Figure 2. (a) Density profile at 710 eV, taken inside the orange box of figure 1(b). (b) Corresponding magnetic profile taken by subtracting and normalizing two images with different helicity of the x-ray beam. The external field, applied perpendicular to the sample plane, is tuned to 0 mT, however the finite stray field of the YIG lamella is also present. Subsequently, the superconductor is field cooled through the superconducting phase transition to a temperature of 26 K. (c)–(e) Area inside the black rectangle after field cooling in magnetic fields of (c) −1 mT, (d) 0 mT and (e) 2 mT. Two confined spots with full but reversed XMCD signal appear at the DW (white line) separating two extended magnetic domains tilted by ±30° OOP.

inhomogeneities in the density landscape (see polarization averaged STXM image in figure 2(a) and in the overall magnetization. We observe a clear shift of the position of both the ferrimagnetic DW and the distinct circular-shaped maxima for different applied fields (see figure 2). The position independent separation and magnetic contrast, where no correlation with the morphological density profile was indicated, exclude a microstructural origin of the observed phenomena. Therefore we can explain the findings to a tightly bound state consisting of a vortex (blue) and an antivortex (red) that is introduced by the interaction between the two vortices itself as well as the interaction between the individual vortex/antivortex and the DW.

Knowing that $\Phi_0 = 2 \times 10^{-15}$ Tm^2 and $B = n\Phi$ where n is the number of vortices per surface unit, it is expected that in general about 0.5 $\frac{\text{vortex}}{\mu\text{m}^2\ \text{mT}}$ are formed inside a field-cooled superconductor. Therefore, the probability that a vortex is formed in the vicinity of the DW coincides with the fact that only one V–AV pair is found along the DW in the field of view of $2 \times 5\ \mu$m^2.

To study the characteristics of this vortex pair in more detail we separate their signal from the ferrimagnetic domain background. For that purpose, the ferrimagnetic structure is modeled using an arctangent function with a DW width of $d_{\text{DW}} = 120$ nm as a fitting parameter. The pair appears as two symmetrically ordered vortices with elliptical shape, (figures 3(a)–(c)) with an individual diameter $w_{x,\text{V}} \approx w_{x,\text{AV}} \approx 240 \pm 15$ nm (FWTM definition). Line profiles in x-direction (figure 3(d)) reveal that both magnetic features have a maximum XMCD contrast of ±14% corresponding to a full local OOP polarization of the YIG sensor layer. Along the DW [y-direction; figure 3(e)] the vortex diameter is compressed to $w_y \approx 145 \pm 15$ nm with a spacing of $s_y \approx 90 \pm 10$ nm between the two vortex cores.

The measured radius $w_x/2 \approx 120 \pm 8$ nm is in good agreement with the London penetration depth $\lambda_{\text{L}} \approx 150$ nm in the *ab*-plane of YBCO. The magnetic flux of a vortex is found by integrating the magnetic flux density $B_{\text{Vortex}}(x) = \frac{\phi_0}{2\pi\lambda\varepsilon} * \text{Bessel}K_0(x)$, with the modified Bessel-function of the second kind zero order Bessel$K_0(x)$, over the area of the imaged vortices. We find a magnetic flux of $0.90 \pm 0.03\ \phi_0$ per vortex, in good accordance with the value of a single magnetic flux quantum. We attribute the slight, but

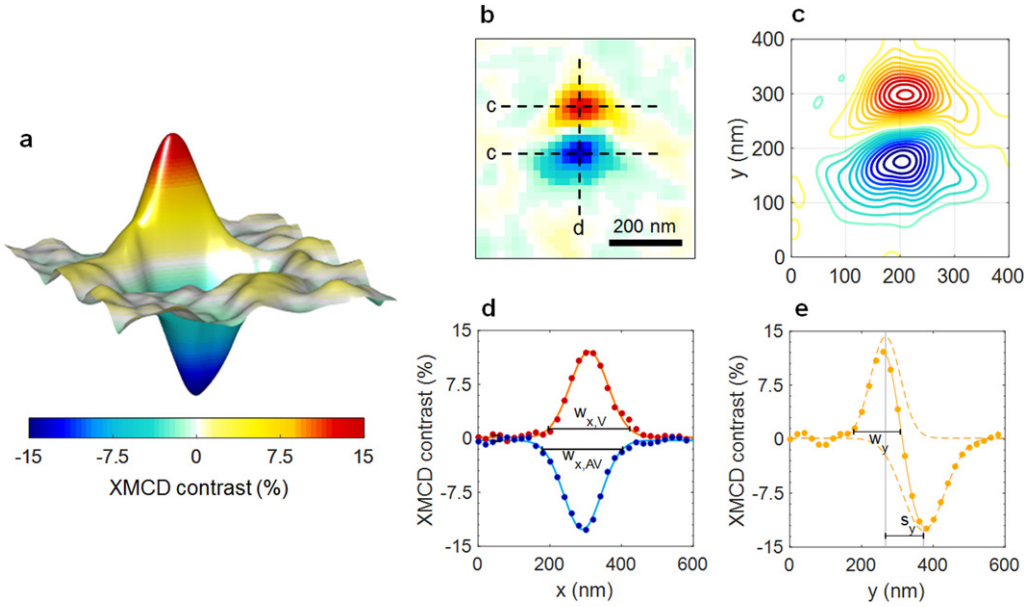

Figure 3. (a) Three-dimensional representation of the experimentally observed V–AV-pair. The XMCD contrast is proportional to the OOP magnetization. The bipolar nature of the V–AV pair can clearly be observed. (b) Background (domain) removed signal of the vortex (red) and antivortex (blue). (c) Contour line plot of the V–AV pair highlighting the compression of the V–AV-pair. (d + e) Line profiles are extracted in *x*-direction (d) and *y*-direction (e), respectively.

experimentally significant difference of $0.10\pm 0.03\ \phi_0$ to the binding energy of the V–AV pair. Following the perspective of the reduced magnetic flux, the binding energy of the V–AV pair can be estimated based on the vortex self-energy E_{Vortex}.

The self-energy of a vortex is described within the Ginzburg–Landau (GL) theory for the free enthalpy. This approach leads to a vortex self-energy in the YBCO film of [31]:

$$E_{\mathrm{Vortex}} = \left(\frac{\phi_0}{4\pi\lambda}\right)^2 * \left(\ln\left[\frac{\lambda}{\xi}\right] + 0.5\right) * d_{\mathrm{YBCO}}.$$

Hence, the reduced magnetic flux of the vortices in the V–AV pair leads to a reduction of the vortex self-energy $\Delta E_{\mathrm{Vortex}} = 36 \pm 10$ eV, which can be used as a measure for the binding energy of the V–AV pair.

For a quantitative description of the V–AV pair formation below T_c and the observed state at $T = 26$ K the forces acting on the vortices have to be balanced by three dominant forces in our experiment: (i) the attractive magnetic interaction force F_{mag} of vortex and antivortex, (ii) the repulsive force $F_{\mathrm{V\text{-}DW}}$ of the DW on the vortices and, (iii) the pinning force F_{pin} in the YBCO film.

The V–AV interaction can be described by a GL ansatz to be

$$F_{\mathrm{mag}} = \frac{\phi_0^2 d_{\mathrm{YBCO}}}{2\pi\lambda^3\mu_0} * \mathrm{Bessel}K_1\left(\frac{s_y}{\lambda(T)}\right), \quad \text{with} \quad \lambda(T) = \lambda_0\left(1 - \left(\frac{T}{T_c}\right)^4\right)^{-\frac{1}{2}},$$

with BesselK_1 as the modified Bessel-function of the second kind first order and the standard temperature dependence of the two-fluid model [32].

The repulsive interaction is given by the derivative of the potential energy$E_{\mathrm{pot}} = -m_{\mathrm{V}} \cdot B_{\mathrm{YIG}}(x)$ of a magnetic dipole in the magnetic flux density $B_{\mathrm{YIG}}(x)$ provided by the ferrimagnetic YIG. The magnetic moment m_{V} of the vortex for a 250 nm YBCO layer corresponds to $8,6 \times 10^8$ Bohr magnetons.

On this basis we calculate the derivative of E_{pot} and find a temperature dependent repulsion of the DW. Figure 4(a) depicts F_{mag} (red line) and $F_{\mathrm{V\text{-}DW}}$ (green line) for the observed V–AV distance $s_y = 90$ nm in the temperature range from 23 K to T_c. We find an equilibrium of forces at about $T = 81$ K.

For the explanation of the experimental result obtained at $T = 26$ K the pinning force on individual vortices in the YBCO film has to be taken into account. Figure 4(b) compares the difference between F_{mag} and $F_{\mathrm{V\text{-}DW}}$ with the pinning force on individual vortices. The latter is extracted from the temperature dependent critical current density $j_c(T)$ via

$$F_{\mathrm{pin}} = j_c(T) * \phi_0 * d_{\mathrm{YBCO}}.$$

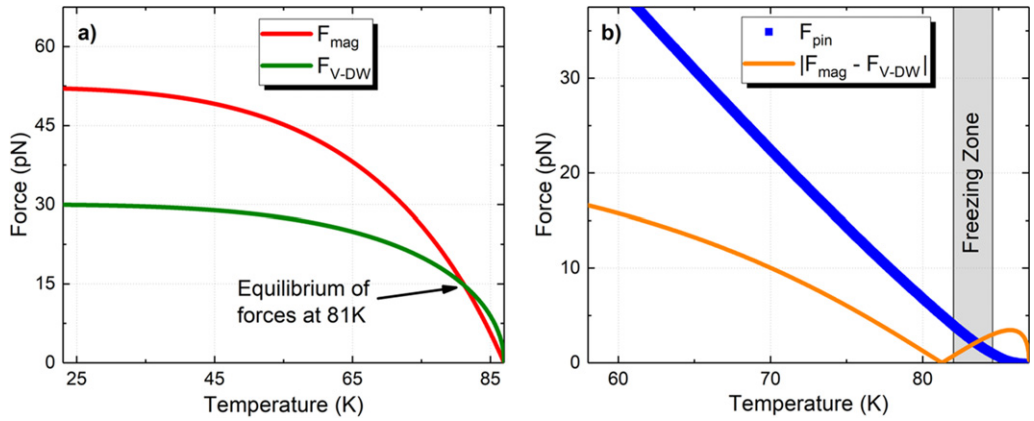

Figure 4. (a) V–AV attraction F_{mag} (red line) and DW repulsion $F_{\mathrm{V\text{-}DW}}$ (green line) forces versus temperature for a V–AV pair with a distance of $d = 90$ nm. Equilibrium of forces is found at $T = 81$ K leading to a bound state. (b) Difference of the interaction forces $|F_{\mathrm{mag}} - F_{\mathrm{V\text{-}DW}}|$ (orange line) compared to the individual vortex pinning force F_{pin} (blue line) in the YBCO film. Below a 'freezing zone' (gray area) at around $T = 83$ K vortex motion is inhibited.

At temperatures below the equilibrium at $T = 81$ K the pinning force is always dominant compared to the interaction forces.

We propose a logic scenario: while cooling the superconductor below T_c vortices of different polarity nucleate in alignment with the stray field directions of the ferrimagnet. Attractive and repulsive forces within the system lead to a bound and stable V–AV state with a temperature dependent binding length. With further reduced temperature the configuration freezes and vortex movement is inhibited by pinning forces. Thus, the measurement at $T = 26$ K provides a snap-shot at the pair-forming temperature around $T = 81$ K. The required inhomogeneous magnetic field [12, 33–35] is achieved by the adjacent DW of the ferrimagnetic system.

Our assumption of a bound and stable V–AV pair is underpinned by a theoretical description found in Laiho *et al* [36]: DWs can induce the nucleation of straight V–AV structures or superconducting semi-loops. Cutting and recombination of semi loops are analyzed in detail in reference [37]. Here, the latter can be excluded due to strong pinning properties and the penetration depth in z-direction being much larger than the thickness of the YBCO layer. This pair formation process is accounted for in Chaves *et al* [38] by the interaction potential in bulk type-II superconductors calculated within the GL theory.

In order to derive the inter-vortex potential, they start from an ansatz with two separate vortices attracting each other as a function of the distance between them. At a critical value dE, the solution with well-defined supercurrents around both vortex and antivortex ceases to be the lowest energy state of the system. In case of thin YBCO films ($\lambda_{\mathrm{L}} \approx 150$ nm, $\xi \approx 1.6$ nm) the stable separation distance d_{E} is $\sim 0.6\ \lambda$ in excellent agreement with our measured V–AV spacing $s_y \approx 90$ nm (see figure 3(e)).

In conclusion, we were able to directly image individual and stable bound V–AV pairs in a high-temperature superconducting thin film. A new variant of scanning magnetic soft x-ray microscopy was used, whereby a spatially decoupled soft YIG layer acts as a sensor layer as well as a source for sufficient and well defined local magnetic field gradients. The nucleation of the V–AV pair occurs at temperatures close to T_c and is observed within the DW of the adjacent ferrimagnet. Owing to the attractive magnetic dipole interaction between V and AV as well as the repulsive force between DW and vortices a highly stable bound V–AV pair is formed. We present a novel experimental access as a stable ground state of a bound particle-antiparticle-like system, which—to our knowledge—has never been observed so far. The results open up a new approach for elucidating vortex physics in type-II superconductors and their interaction with external magnetic fields. The potential of the STXM method, which allow also an elemental specific mapping of the sample morphology with high contrast allows to correlate flux pinning to chemical landscapes which is highly relevant for modern HTc materials with high critical current densities [39]. In addition, the experimental x-ray based techniques provide a new approach for nm scale stray-field imaging with high contrast. Using the STXM possibilities for picosecond time resolution and target excitations by magnetic fields, currents and voltage pulses, even a dynamical access [40] is possible that offers even extended possibilities compared to results from dynamical SQUID-on-tip microscopy [41]. Hereby, also V–AV interaction and their interplay with time-dependent external magnetic fields and also spin waves, created in a dynamically active sensor layer, could be addressed.

Author contribution

All authors contributed extensively to the work presented in this paper. JS fabricated the samples, performed the experiment, analyzed and interpreted the data and prepared the manuscript; MB performed the experiment and analyzed the data; AI performed the experiment and prepared the manuscript; MW gave technical support and conceptual advice; GS and JA developed the concept, interpreted the data and prepared the manuscript.

Acknowledgment

The authors are grateful to U Eigenthaler, B Stuhlhofer and T Meisner (MPI Stuttgart) for their contributions to the sample fabrication.

ORCID iDs

A M Ionescu https://orcid.org/0000-0001-7357-4249
J Albrecht https://orcid.org/0000-0002-4047-4302

References

[1] Mermin N D 1979 The topological theory of defects in ordered media *Rev. Mod. Phys.* **51** 591–648
[2] van Waeyenberge B *et al* 2006 Magnetic vortex core reversal by excitation with short bursts of an alternating field *Nature* **444** 461–4
[3] Yadav A K *et al* 2016 Observation of polar vortices in oxide superlattices *Nature* **530** 198–201
[4] Berdiyorov G R, Milošević M V, Covaci L and Peeters F M 2011 Rectification by an imprinted phase in a Josephson junction *Phys. Rev. Lett.* **107** 177008
[5] Golod T, Iovan A and Krasnov V M 2015 Single Abrikosov vortices as quantized information bits *Nat. Commun.* **6** 8628
[6] Kosterlitz J M and Thouless D J 1973 Ordering, metastability and phase transitions in two-dimensional systems *J. Phys. C: Solid State Phys.* **6** 1181–203
[7] Beasley M R, Mooij J E and Orlando T P 1979 Possibility of vortex–antivortex pair dissociation in two-dimensional superconductors *Phys. Rev. Lett.* **42** 1165
[8] Kim D H, Goldman A M, Kang J H and Kampwirth R T 1989 Kosterlitz–Thouless transition in $Tl_2Ba_2CaCu_2O_8$ thin films *Phys. Rev.* B **40** 8834
[9] Benfatto L, Castellani C and Giamarchi T 2009 Broadening of the Berezinskii–Kosterlitz–Thouless superconducting transition by inhomogeneity and finite-size effects *Phys. Rev.* B **80** 214506
[10] Lange M, van Bael M J, Silhanek A V and Moshchalkov V V 2005 Vortex–antivortex dynamics and field-polarity-dependent flux creep in hybrid superconductor/ferromagnet nanostructures *Phys. Rev.* B **72** 052507
[11] Neal J S, Milošević M V, Bending S J, Potenza A, San Emeterio L and Marrows C H 2007 Competing symmetries and broken bonds in superconducting vortex–antivortex molecular crystals *Phys. Rev. Lett.* **99** 127001
[12] Chibotaru L F, Ceulemans A, Bruyndoncx V and Moshchalkov V V 2000 Symmetry-induced formation of antivortices in mesoscopic superconductors *Nature* **408** 833–5
[13] Milošević M V and Peeters M 2003 Superconducting Wigner vortex molecule near a magnetic disk *Phys. Rev.* B **68** 024509
[14] Milošević M V and Peeters F M 2005 Vortex–antivortex nucleation in magnetically nanotextured superconductors: magnetic-field-driven and thermal scenarios *Phys. Rev. Lett.* **94** 227001
[15] Stolyarov V S *et al* 2018 Domain Meissner state and spontaneous vortex–antivortex generation in the ferromagnetic superconductor $EuFe_2(As_{0.79}P_{0.21})_2$ *Sci. Adv.* **4** 1061
[16] Wells F S, Pan A V, Wang X R, Fedoseev S A and Hilgenkamp H 2015 Analysis of low-field isotropic vortex glass containing vortex groups in $YBa_2Cu_3O_{7-x}$ thin films visualized by scanning SQUID microscopy *Sci. Rep.* **5** 8677
[17] Iavarone M, Scarfato A, Bobba F, Longobardi M, Karapetrov G, Novosad V, Yefremenko V, Giubileo F and Cucolo A M 2011 Imaging the spontaneous formation of vortex–antivortex pairs in planar superconductor/ferromagnet hybrid structures *Phys. Rev.* B **84** 024506
[18] Lange M, Bael M J V, Bruynseraede Y and Moshchalkov V V 2003 Nanoengineered magnetic-field-induced superconductivity *Phys. Rev. Lett.* **90** 197006
[19] Bending S J, Neal J S, Milošević M V, Potenza A, San Emeterio L and Marrows C H 2008 Competing symmetries in superconducting vortex–antivortex 'molecular crystals' *Phys.* C **468** 518–22
[20] Thiel L, Rohner D, Ganzhorn M, Appel P, Neu E, Müller B, Kleiner R, Koelle D and Maletinsky P 2016 Quantitative nanoscale vortex imaging using a cryogenic quantum magnetometer *Nat. Nanotechnol.* **11** 677–81
[21] Harada K *et al* 1992 Real-time observation of vortex lattices in a superconductor by electron microscopy *Nature* **360** 51–3
[22] Harada K 2013 Lorentz microscopy observation of vortices in high-T_c superconductors using a 1 MV field emission transmission electron microscope *J. Electron Microsc.* **62** 3–15
[23] Liu W *et al* 2020 A new Majorana platform in an Fe-As bilayer superconductor *Nat. Commun.* **11** 5688
[24] Guillamón I, Suderow H, Fernández-Pacheco A, Sesé J, Córdoba R, De Teresa J M, Ibarra M R and Vieira S 2009 Direct observation of melting in a two-dimensional superconducting vortex lattice *Nat. Phys.* **5** 651–5
[25] Liu W *et al* 2016 Evidence for ferromagnetic coupling at the doped topological insulator/ferrimagnetic insulator interface *AIP Adv.* **6** 055813
[26] Stahl C *et al* 2014 Detecting magnetic flux distributions in superconductors with polarized x-rays *Phys. Rev.* B **90** 104515

[27] Simmendinger J, Ruoss S, Stahl C, Weigand M, Gräfe J, Schütz G and Albrecht J 2018 Transmission x-ray microscopy at low temperatures: irregular supercurrent flow at small length scales *Phys. Rev.* B **97** 134515
[28] Simmendinger J, Weigand M, Schütz G and Albrecht J 2020 Magnetic flux penetration into micron-sized superconductor/ferromagnet bilayers *Supercond. Sci. Technol.* **33** 025015
[29] Simmendinger J *et al* 2019 Magnetically induced anisotropy of flux penetration into strong-pinning superconductor/ferromagnet bilayers *New J. Phys.* **21** 113019
[30] Mayer J, Giannuzzi L A, Kamino T and Michael J 2007 TEM sample preparation and FIB-induced damage *MRS Bull.* **32** 400–7
[31] Brandt E H 1995 The flux-line lattice in superconductors *Rep. Prog. Phys.* **58** 1465–594
[32] Kittel C 2004 *Introduction to Solid State Physics* (New York: Wiley)
[33] Milošević M V and Peeters F M 2004 Vortex–antivortex lattices in superconducting films with magnetic pinning arrays *Phys. Rev. Lett.* **93** 267006
[34] Priour D J and Fertig H A 2004 Vortex states of a superconducting film from a magnetic dot array *Phys. Rev. Lett.* **93** 057003
[35] Lima C L S and De Souza Silva C C 2009 Dynamics of vortex–antivortex matter in nanostructured ferromagnet-superconductor bilayers *Phys. Rev.* B **80** 054514
[36] Laiho R, Lähderanta E, Sonin E B and Traito K B 2003 Penetration of vortices into the ferromagnet/type-II superconductor bilayer *Phys. Rev.* B **67** 144522
[37] Berdiyorov G R, Doria M M, Romaguera A R D C, Milošević M V, Brandt E H and Peeters F M 2013 Current-induced cutting and recombination of magnetic superconducting vortex loops in mesoscopic superconductor-ferromagnet heterostructures *Phys. Rev.* B **87** 184508
[38] Chaves A, Peeters F M, Farias G A and Milošević M V 2011 Vortex–vortex interaction in bulk superconductors: Ginzburg–Landau theory *Phys. Rev.* B **83** 054516
[39] Jha A K and Matsumoto K 2019 Superconductive REBCO thin films and their nanocomposites: the role of rare-earth oxides in promoting sustainable energy *Front. Physiol.* **7** 1–12
[40] Litzius K *et al* 2020 The role of temperature and drive current in skyrmion dynamics *Nat. Electron.* **3** 30–6
[41] Embon L *et al* 2017 Imaging of super-fast dynamics and flow instabilities of superconducting vortices *Nat. Commun.* **8** 85